A&A 390, 289–298 (2002)
DOI: 10.1051/0004-6361:20020710

Astronomy & Astrophysics

CH_3OH and H_2O masers in high-mass star-forming regions

H. Beuther[1], A. Walsh[1], P. Schilke[1], T. K. Sridharan[3], K. M. Menten[1], and F. Wyrowski[1]

[1] Max-Planck-Institut für Radioastronomie, Auf dem Hügel 69, 53121 Bonn, Germany
[2] Harvard-Smithsonian Center for Astrophysics, 60 Garden Street, MS 78 Cambridge, MA 02138, USA

Received 31 October 2001 / Accepted 7 May 2002

Abstract. We present a comparison of Class II CH_3OH (6.7 GHz) and H_2O (22.2 GHz) masers at high spatial resolution in a sample of 29 massive star-forming regions. Absolute positions of both maser types are compared with mm dust continuum, cm continuum and mid-infrared sources. All maser features – regardless of the species – are associated with massive mm cores, but only 3 out of 18 CH_3OH masers and 6 out of 22 H_2O masers are associated with cm emission likely indicating the presence of a recently ignited massive star. These observations of a homogenous sample of massive, young star-forming regions confirm earlier results, obtained for each maser species separately, that both maser types are signposts of high-mass star formation in very early evolutionary stages. The data are consistent with models that explain CH_3OH maser emission by radiative pumping in moderately hot cores, requiring the absence, or only weak, free-free cm continuum radiation due to recently ignited stars. Mid-infrared sources are associated with both maser types in approximately 60% of the observed fields. Thus, mid-infrared objects may power maser sites, but the detection of strong mid-infrared emission is not strictly necessary because it might be heavily extincted. A comparison of the spatial separations between the different observed quantities and other properties of the star-forming regions does not reveal any correlation. Our data suggest that CH_3OH and H_2O masers need a similar environment (dense and warm molecular gas), but that, due to the different excitation processes (radiative pumping for CH_3OH and collisional pumping for H_2O), no spatial correlations exist. Spatial associations are probably coincidences due to insufficient angular resolution and projection effects. The kinematic structures we find in the different maser species show no recognizable pattern, and we cannot draw firm conclusions as to whether the features are produced in disks, outflows or expanding shock waves.

Key words. masers – stars: formation – ISM: dust, extinction – ISM: jets and outflows – infrared: ISM – radio continuum: ISM

1. Introduction

Over the last decade, it has become clear that Class II CH_3OH and H_2O maser emission is closely associated with the earliest stages of massive star formation. Much research has been focused on both maser species, but most high-resolution studies have concentrated on only one type. Little is known about the associations and connections of the CH_3OH and the H_2O maser emission. Motivated by this lack of information, we conducted high-resolution observations of both maser types in a large sample of high-mass protostellar objects (HMPOs) and discuss them in the context of different other probes of massive star formation.

So far, high-resolution investigations, focused either on H_2O or on CH_3OH maser emission, indicate independently that both maser types are found in outflows as well as in circumstellar disks. Examples of these studies on the H_2O side are, e.g., Torrelles et al. (1997, 1998), Codella & Felli (1995), and Codella et al. (1996, 1997), whereas recent studies of CH_3OH masers include Walsh et al. (1997, 1998), Phillips et al. (1998), Minier et al. (2000a, 2001), and Codella & Moscadelli (2000). Reviews on this subject are found in Menten (1996), Garay & Lizano (1999), Norris (2000), and Kylafis & Pavlakis (1999).

Another finding is that both maser types are occasionally spatially coincident with ultracompact HII regions, but more often with hot molecular cores and/or massive molecular outflows (Hofner & Churchwell 1996; Codella et al. 1996, 1997; Walsh et al. 1998; Garay & Lizano 1999; Minier et al. 2001). Recent studies by Walsh et al. (2001) indicate that CH_3OH masers often are associated with mid-infrared sources that should be luminous enough to produce strong ionizing radiation. In spite of that, a number of those maser sites is undetected in the radio continuum, and Walsh et al. (2001) conclude that these might be in an evolutionary stage prior to forming an ultracompact HII region.

For sources in which both maser species are observed (mostly single-dish data with low spatial resolution), the velocity spread is far higher in the case of H_2O maser emission than known for CH_3OH masers. For example, Sridharan et al. (2002) found in a sample of high-mass protostellar

Send offprint requests to: H. Beuther,
e-mail: beuther@mpifr-bonn.mpg.de

candidates that the CH_3OH emission is confined always to a total radial velocity extent of at most 15 km s^{-1}, whereas the H_2O maser emission is found extending up to 70 km s^{-1}. In spite of the similarities outlined above, these different spectral features show that the two maser types are subject to different excitation conditions and likely occur in separate spatial regions around the evolving massive protostars.

The current status of CH_3OH maser excitation studies favors a scenario in which the CH_3OH maser emission is produced by radiative pumping in small, moderately hot regions ($\sim$150 K) with CH_3OH column densities $>10^{15}$ cm^{-2} and hydrogen number densities $<10^8$ cm^{-3} (Hartquist et al. 1995; Sobolev et al. 1997; Cragg et al. 2001). While it was suggested that CH_3OH maser could be produced in disks (e.g., Norris et al. 1998), this is not unambiguously confirmed, and other scenarios like expanding shock waves or outflows have been proposed as well (e.g., Walsh et al. 1998; Minier et al. 2000b). It is quite possible that the same maser species in different sources have different origins.

In contrast, most H_2O maser models explain the excitation by collisional pumping with H_2 molecules within shocks associated with outflows and/or accretion (Elitzur et al. 1989; Garay & Lizano 1999). For example, the model by Elitzur et al. (1989) requires dissociative shocks in dense gas (preshock densities around 10^7 cm^{-3}) with temperatures up to $\sim$400 K. In many sources, it is believed that the H_2O masers form within outflows, but there are also examples claiming that the H_2O masers are produced in disks (Garay & Lizano 1999).

The high-resolution study of H_2O and CH_3OH maser emission in 29 high-mass star-forming regions presented here intends to compare the characteristics of these important signposts of massive star formation. The study is part of a long-term project studying very early evolutionary stages of massive star formation, prior to, or during the formation of an ultracompact HII region. The entire sample of 69 sources presented first by Sridharan et al. (2002) is distributed mainly between 1 kpc and 10 kpc distance from the sun. For many sources, only kinematic distances are known, and the data suffer from the distance ambiguity of this approach (Sridharan et al. 2002). The bolometric luminosities of the sources range roughly between $10^{3.5}$ $L_\odot$ and $10^{5.6}$ $L_\odot$, and the core masses vary between a few 100 $M_\odot$ and a few 10^4 $M_\odot$. Detailed analyzes of different sample properties (luminosities, density distributions, outflows) are presented in Sridharan et al. (2002) and Beuther et al. (2002a, b). In spite of the non-detection in Galaxy-wide single-dish cm surveys, more sensitive interferometric studies revealed that in some of the sources cm emission occurs, whereas in others we do not find any free-free emission down to 1 mJy. This makes the sample ideally suited for the study of associations of masers with different kinds of sources and evolutionary stages. The basic source properties of the sub-sample analyzed in this paper are summarized in Table 1. We compare the maser emission mainly with mm dust emission tracing the massive core (Beuther et al. 2002a), cm wavelength emission being believed to be due to free-free emission in those sources where it had been detected (Sridharan et al. 2002), and mid-infrared emission likely due to warm dust around embedded objects.

2. Observations

2.1. Single-dish H_2O and CH_3OH maser data

An H_2O (22.2 GHz) and Class II CH_3OH Class (6.7 GHz) maser survey of the the whole sample of 69 high-mass protostellar objects, as introduced by Sridharan et al. (2002), was conducted with the Effelsberg 100 m telescope in two runs in 1998. Altogether, 29 H_2O and 26 CH_3OH masers were found. The observations are described and statistically analyzed in Sridharan et al. (2002). Follow-up observations of the maser detections were conducted with high spatial resolution with the VLA and the ATCA.

2.2. H_2O maser observations with the VLA

High-resolution images of the 22.2 GHz H_2O maser line were obtained with the Very Large Array (VLA) in the B configuration with a spectral resolution of 0.65 km s^{-1}, a synthesized HPBW of $\approx$0.4″, and a primary beam *FWHM* of $\approx$2′. The snapshot mode was used with 3×5 min integrations spread over the transit of each source. We reduced the data with the AIPS software package using standard procedures. The typical 1σ sensitivity is 1 Jy.

For 22 out of 26 observed sources, the signal-to-noise ratio and the UV coverage were sufficiently good to derive absolute positions to an accuracy better than 1″. The accuracy of relative positions of different maser features is around 0.1″.

2.3. CH_3OH maser observations with the ATCA

To get high-resolution images of the Class II 6.7 GHz maser line of CH_3OH, we employed the Australian Telescope Compact Array (ATCA) which is part of the Australia Telescope National Facility. From the 26 sources initially found to be associated with CH_3OH maser emission, 21 are south of declination 20° which is necessary to be observable with the ATCA. Six of the 21 sources had already been observed with the ATCA by Walsh et al. (1998). Thus, we observed the remaining 15 objects in the snapshot mode with a series of 6 short integration cuts of 5 min for each source. Phase calibrators were observed every 20 min. The field of view of the ATCA at this frequency is $\sim(8')^2$, and the effective HPBW of the synthesized beam is $\sim$1.9″. Observations near the equator result in elongated, elliptical beams because of the east–west elongation of the array. The spectral resolution was $\sim$0.2 km s^{-1}, and the 1σ sensitivity was typically 0.5 Jy.

In 10 out of the 15 sources the data are sufficiently good to derive positions. The data reduction was performed with the MIRIAD software package using standard procedures. Absolute positions are estimated to be accurate to 1″ whereas the relative positions should be accurate to $\sim$0.1″. In 4 sources the signal was too weak to be detected, whereas in 1 source the signal was strong enough, but so close to the equator that no positions could be derived.

2.4. Other observations

Dust emission at mm wavelengths
The 29 sources presented in this paper were observed as part of the large sample of 69 high-mass protostellar objects introduced by Sridharan et al. (2002) with the MAMBO array in the 1.2 mm continuum. A detailed description of the data reduction and analysis can be found in Beuther et al. (2002b). For a few sources even higher resolution mm data were obtained with the Plateau de Bure Interferometer and the BIMA array at 2.6 mm. Plateau de Bure data are used here for 05358+3543 and 19217+1651, whereas the BIMA data were used in the cases of 18089 – 1733, 18264 – 1152, 18566+0408 and 23033+5951. Details of the Plateau de Bure observations are presented in Beuther et al. (2002c) and Beuther et al. (in prep.), and the BIMA observations will be published by Wyrowski et al. (in prep.).

The pointing accuracy of the MAMBO array is estimated to be around 5″ and the BIMA and Plateau de Bure data should be accurate to approximately 1″.
Continuum emission at cm wavelengths, likely produced by free-free emission
To know whether faint cm emission is present in some of the sources, we obtained 3.6 cm continuum images with the VLA down to a 1σ sensitivity of 0.1 mJy with a spatial resolution of 0.7″. For more details see Sridharan et al. (2002). The positions of these data are correct to within 1″.
Mid-infrared data
The Midcourse Space Experiment (MSX) point source catalog was searched for mid-infrared sources in the respective fields of view. For details on MSX see, e.g., Egan et al. (1998) and the MSX Web site[1]. In most fields, mid-infrared sources were found (Sridharan et al. 2002). For the few sources, for which the point source catalog had no entries, we examined the most sensitive MSX images at 8 μm and extracted source positions. The spatial resolution of MSX is approximately 18″, and the sensitivity varies between the different bands between 0.1 and 30 Jy/beam. Egan et al. (1998) quote the positions to be accurate within 4″–5″. For 05358+3543, we use a mid-infrared source position observed by McCaughrean et al. (in prep.) with the Keck observatory at 11.7 μm.

3. Results

3.1. The database

Figure 1 presents maps of the 29 maser sources observed with high spatial resolution. For 6 sources the CH_3OH data are taken from Walsh et al. (1998), for 19410+2336 the CH_3OH maser positions are presented by Minier et al. (2000a), and for 05358+3543 no high-resolution CH_3OH maser position is known (single dish detection by, e.g., Sridharan et al. 2002 and Menten Menten 1991). Of the 6 sources in our sample north of 20° declination, Effelsberg 100 m data show that three (19410+2336, 20126+4104 & 23139+5939) contain CH_3OH masers (Table 1), but because the ATCA is only capable of observing sources below 20° declination, we have accurate CH_3OH maser positions only for 19410+2336 and 20126+4104, both of which were observed with the European VLBI network (EVN) by Minier et al. (2000a, 2001). Table 2 lists the positions of the maser features.

As we want to understand what kind of source is powering the masers, Fig. 1 also shows other features characterizing the massive star-forming regions:
(1) mm dust continuum data, tracing the massive molecular cores in which the stars form,
(2) mid-infrared data, indicating warm dust around an embedded protostar,
(3) and cm continuum emission, probably due to optically thin free-free emission signposting recently ignited massive stars belonging to the same cluster. But as we do not have spectral index information in the cm regime, it is also possible that some of the cm features are still optically thick or could be due to jets (see also Sridharan et al. 2002).

Table 1 presents more characteristic source properties, such as the total luminosities, distances and core masses (Sridharan et al. 2002; Beuther et al. 2002a).

It is of major interest to see how the different maser types are associated with other observable features. Because of the positional accuracy of the maser and cm observations of ≈1″, we cannot reliably separate features that are closer than 1.5″ to each other. On linear scales at the given distances of a few kpc, this is still a large separation (e.g., at 4 kpc distance, 1.5″ correspond to ≈6000 AU ≈0.03 pc), and we cannot be certain whether sources within 1.5″ of each other are associated or not. It has also to be taken into account that those separations are projections on the plane of the sky, and there are probably spatial offsets along the line of sight as well. If more than one maser feature is detected we derived the separations using the nearest positions (except of the H_2O maser spots in 19217+1651 because clearly two different groups exist). Lada (1999) report a mean separation between stellar objects in clusters around 0.1 pc, and McCaughrean & Stauffer (1994) find mean separations in the center of the Orion Nebula Cluster of ~0.03 pc. The scenario of merging intermediate-mass protostars within the innermost center of star-forming cores requires even higher protostellar densities between 10^6 pc^{-3} and 10^8 pc^{-3}, corresponding to mean separations between 0.01 pc and 0.002 pc (Bonnell et al. 1998; Stahler et al. 2000). Taking all these different estimates into account, it is possible that a significant fraction of features, that seem to be associated within our observational accuracy, are powered by the same underlying source, but we cannot be certain, and it is possible that multiple features are powered by separate multiple sources. Within these powering sources, different maser origins are possible, e.g., outflows, disks or expanding shock waves (e.g., Garay & Lizano 1999). Furthermore, separate components of a binary or multiple system might account for the maser emission, because multiple system are more common in high-mass than in low-mass star-forming regions (Preibisch et al. 1999). Due to the lower spatial resolution and lower positional accuracy, mm and mid-infrared sources cannot be separated from the maser features when they are located within 5″.

[1] http://www.ipac.caltech.edu/ipac/msx/msx.html

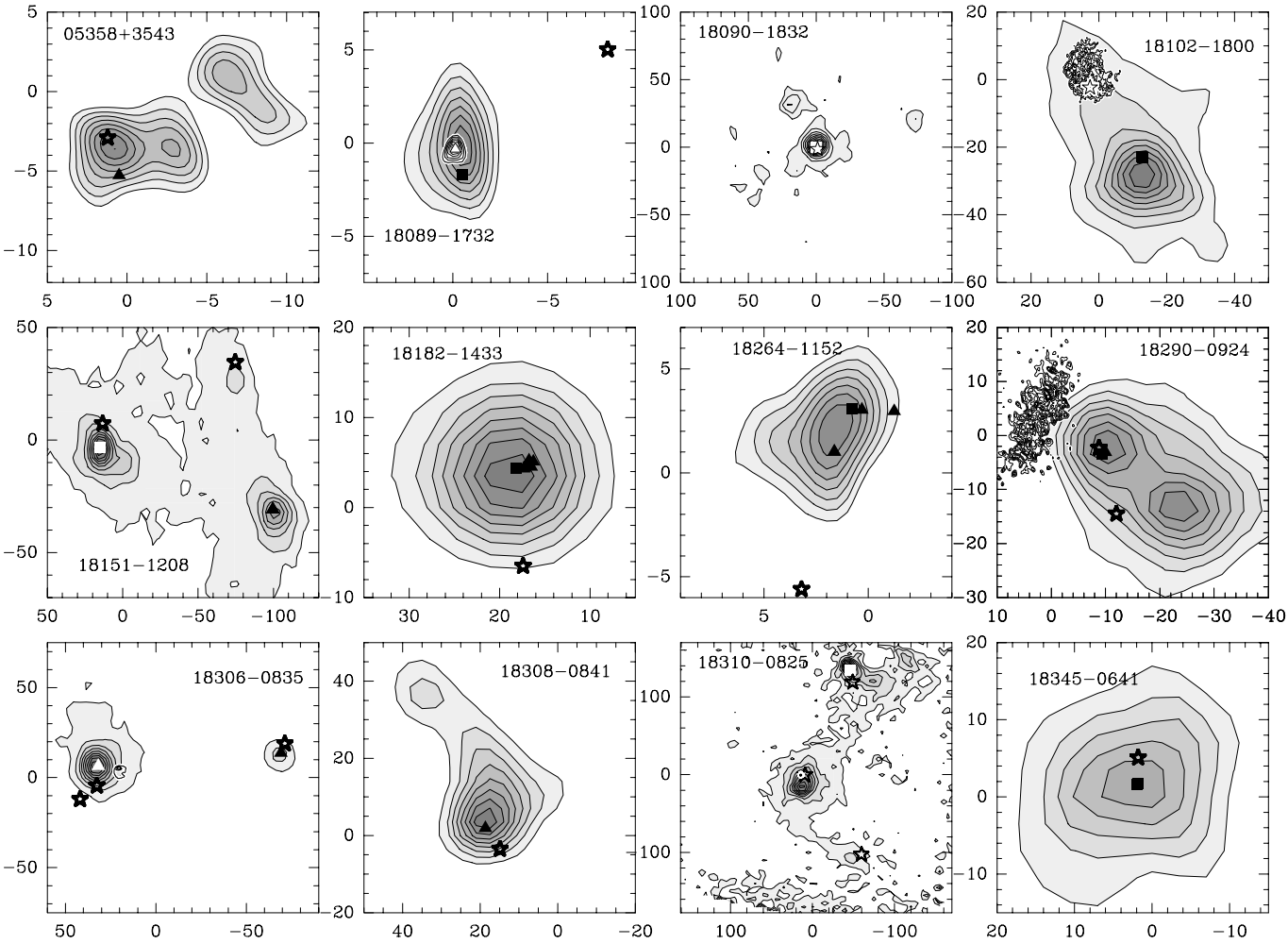

Fig. 1. CH_3OH (squares) and H_2O (triangles) maser positions are presented. The grey-scales with contours show the mm continuum images (thermal dust emission), the black (on white) contours present the cm observations tracing the free-free emission and the stars mark the mid-infrared point source positions. The axes show offsets in arcseconds from the IRAS position with varying scales for the different sources.

As the sample is distributed throughout the whole Galactic disk with largely different distances, we calculate linear separations between the masers and the other observable quantities (mm, cm and mid-infrared emission). For sources, where the separation is below the pointing accuracy of the observations, the derived values have to be taken cautiously because the errors are larger. As we only know kinematic distances for many of the sources, Tables 3 and 4 list the separations derived for the near and the far distance, respectively. Table 5 presents the mean separations; for sources with distance ambiguity we choose the near distance for this calculation. Additionally, a summary of the features which are, within the observing accuracy, associated with each other is given in Table 5.

3.2. Associations and (non-)correlations

Regarding the sources south of declination 20°, which were in the observable range of both telescopes (the ATCA and the VLA), and including 19410+2336 and 20126+4104 (EVN and VLA data from Minier et al. 2000a, 2001), in 11 sources both maser types are detected, in 7 just the CH_3OH masers, and in 6 only the H_2O masers. Thus, ∼38% of the CH_3OH maser sources do not show H_2O maser emission, and ∼35% of the H_2O maser sources do not emit in the CH_3OH maser line. This shows that both maser types could be powered by similar sources, but that finding one does not necessarily imply finding the other as well. It rather confirms significant differences in the emission process as already expected by the different velocity ranges (e.g., Garay & Lizano 1999; Sridharan et al. 2002). As we are dealing with low-number statistics, we estimate the error by $1/\sqrt{N}$ with N being the number of sources we are investigating. Thus, the approximate statistical errors of our analysis are in the 20% range (relative to the percentages of associations and (non-)correlations.) In sources with both maser types, the masers seem to be always associated within the accuracy of 1.5″, except for 18 151−1208, the only field of view where both types are detected but in two separate mm cores, 80″ apart. In contrast, in many sources just one of both maser types is present.

Both maser species are always found close to a mm core, traced by the dust continuum peak, with an average projected separation of 0.03 pc (Table 5). Considering the mean spatial

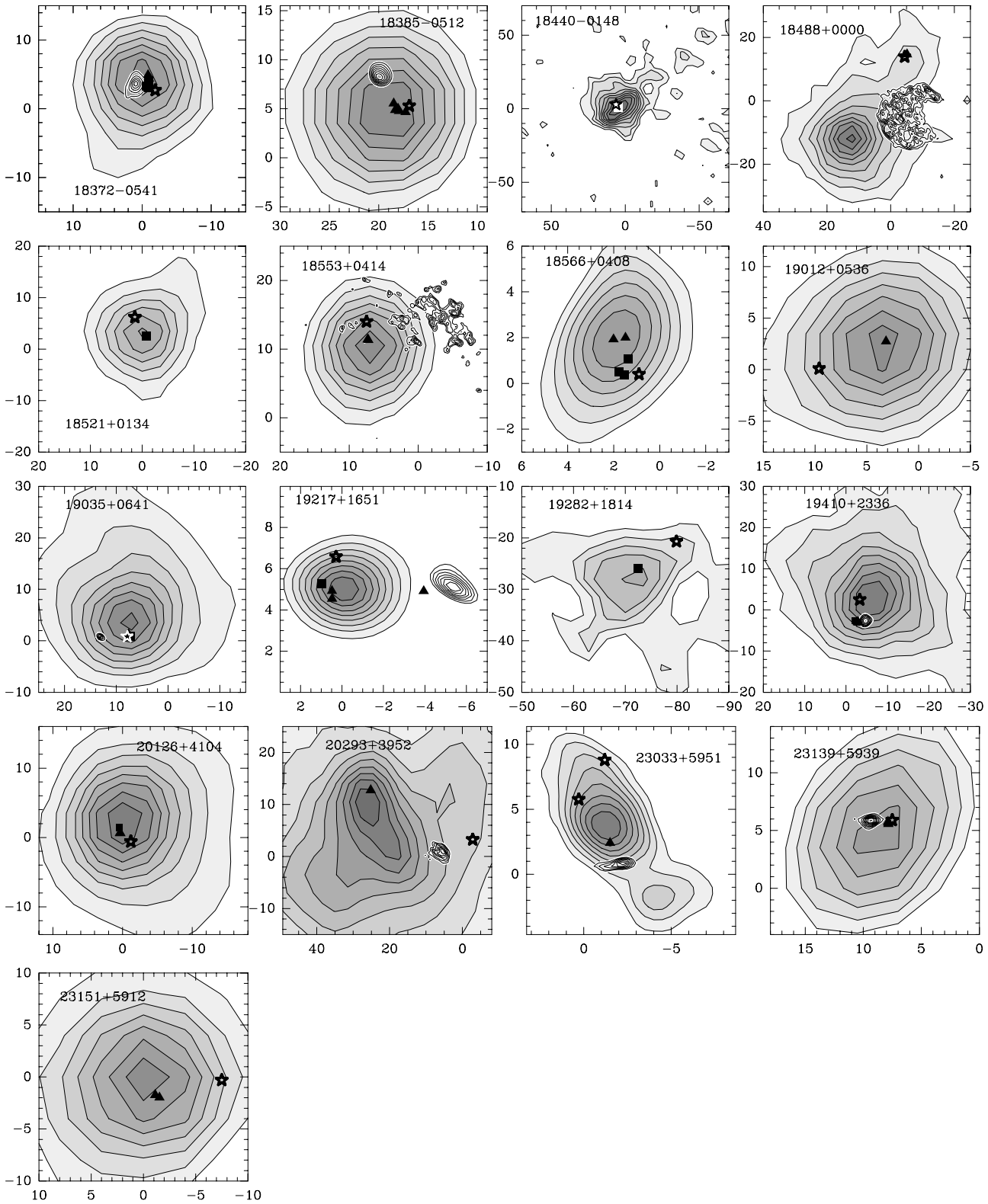

Fig. 1. continued.

separations within star-forming cluster (see 3.1), it is possible that both masers are amplified by the same powering source. Interestingly, 6 out of 22 H_2O masers ($27 \pm 5\%$) are, within the observing accuracy, also associated with cm emission, while only 3 out of 18 CH_3OH masers ($17 \pm 5\%$) are nearby the cm peaks. The statistical difference between both maser–cm associations is only weak. It is quite possible that some of the maser/cm associations are even chance alignments due to projection effects, but we cannot quantify that more precisely. We note that we do not find any source with CH_3OH and cm

Table 1. Characteristic parameters of the maser associated massive star-forming regions. The distances, luminosities, 3.6 cm fluxes and single-dish maser fluxes are taken from Sridharan et al. (2002), the core masses and peak column densities of the main mm core are derived from 1.2 mm dust continuum data (Beuther et al. 2002a). If no near-values are given, the distance ambiguity is solved (Sridharan et al. 2002).

source	d_{far} [kpc]	d_{near} [kpc]	L_{far} [$L_\odot$]	L_{near} [$L_\odot$]	M_{far} [$M_\odot$]	M_{near} [$M_\odot$]	N_{H_2} [10^{23} cm^{-2}]	cm [mJy]	CH_3OH [Jy]	H_2O [Jy]
05358+3543	1.8	–	3.8	–	610	–	5.8	<1	162	45
18089−1732	13.0	3.6	5.6	4.5	31900	2400	17	0.9	54	75
18090−1832	10.0	6.6	4.5	4.1	4600	2000	2.4	?	82	–
18102−1800	14.0	2.6	5.3	3.8	24000	800	2.9	44	9	–
18151−1208	3.0	–	4.3	–	1100	–	4.4	<1	50	0.8
18182−1433	11.8	4.5	5.1	4.3	20700	3000	9.4	<1	24	18
18264−1152	12.5	3.5	5.1	4.0	55300	4300	16	<1	4	50
18290−0924	10.5	5.3	5.0	4.4	6500	1600	3.3	7.0	15	4
18306−0835	10.7	4.9	4.8	4.1	16400	3400	6.9	82	–	0.7
18308−0841	10.7	4.9	4.9	4.2	12800	2700	4.6	<1	–	1.5
18310−0825	10.4	5.2	4.8	4.2	15300	3800	1.8	7.0	–	–
18345−0641	9.5	–	4.6	–	6900	–	2.4	27	5	3
18372−0541	13.4	1.8	5.3	3.5	10200	200	2.6	80	9	1.5
18385−0512	13.1	2.0	5.3	3.7	13400	300	4.5	29	–	200
18440−0148	8.3	–	4.7	–	1700	–	0.4	<1	4	?
18488+0000	8.9	5.4	4.9	4.5	6100	2200	2.9	194	17	1
18521+0134	9.0	5.0	4.6	4.1	3000	900	2.0	<1	1	–
18553+0414	12.9	0.6	5.1	2.4	15800	35	3.6	<1	–	50
18566+0408	6.7	–	4.8	–	2100	–	2.9	<1	7	3
19012+0536	8.6	4.6	4.7	4.2	3900	1100	2.9	<1	1	2
19035+0641	2.2	–	3.9	–	390	–	1.9	4.0	14	9
19217+1651	10.5	–	4.9	–	9500	–	5.3	32	1	9
19282+1814	8.2	1.9	4.9	3.6	2700	150	2.4	<1	3	–
19410+2336	6.4	2.1	5.0	4.0	7800	800	5.7	1	30	110
20126+4104	1.7	–	3.9	–	500	–	5.2	<1	36	15
20293+3952	2.0	1.3	3.8	3.4	500	200	1.9	7.6	–	100
23033+5951	3.5	–	4.0	–	2300	–	3.7	1.7	–	4
23139+5939	4.8	–	4.4	–	1800	–	4.0	1.4	3	400
23151+5912	5.7	–	5.0	–	1200	–	1.8	<1	–	60

emission without an H_2O maser nearby, whereas in three sources H_2O and cm peaks are coincident within our accuracy, but no observed CH_3OH maser is found in the same region. An interesting example, which illustrates the different maser properties, is 19 217+1651: some H_2O and CH_3OH features are associated with the massive mm core, whereas another H_2O feature is found near the cm source approximately 6″ apart (Fig. 1). As the mm data are from interferometric Plateau de Bure observations (accuracy 1″), the separation of the cm and mm peaks is real.

The mid-infrared sources stand somewhere between all the other features. In some cases, they seem to be associated with the mm sources and in other objects with the cm sources. The same is observed for their spatial associations with both maser species, in some sources their positions coincide within the observing accuracy, in others they do not. A very peculiar example is 18 488+0000, where an archetypical cometary ultracompact HII region is at the edge of the mm core, but most surprising, the mid-infrared source as well as the H_2O maser feature do not coincide with any of them, but are located at a small secondary mm peak that looks insignificant from the mm point of view (but is still massive, ∼400 $M_\odot$ at the near kinematic distance of ∼5 kpc, Beuther et al. 2002b).

To get a quantitative understanding of the spatial associations, we tried to find correlations between the linear separations of the different observed tracers and other quantities of our sample (the luminosities, core masses, H_2 column densities and densities, as taken from Sridharan et al. 2002 and Beuther et al. 2002a). We did not find any correlation among all those different quantities.

3.3. Internal maser structure

To investigate whether the maser features show linear or arc-like structures indicative of specific emission regions (disks, outflows, or expanding shock waves, e.g., Walsh et al. 1998; Garay et al. 1999; Norris 2000; Kylafis & Pavlakis 1999; Minier et al. 2000a), we focused on the 6 sources for which we have at least 3 spatially separate maser features in one or both species. Outflows are ubiquitous features in massive star-forming regions (Sridharan et al. 2002; Richer et al. 2000; Churchwell 2000), therefore we additionally present the bipolar outflow directions found by Beuther et al. (2002b). Figure 2 shows the results.

Morphologically, one can find rings, arcs or linear structures in all cases, even between different maser species. But

Table 2. Positions of the CH_3OH & H_2O maser. For the sources with citation we took the CH_3OH maser data from [1]Walsh et al. (1998) and [2]Minier et al. (2000a, 2001).

source	CH_3OH [J2000.0]	v_{LSR} [km s^{-1}]	H_2O [J2000.0]	v_{LSR} [km s^{-1}]
05358+3543	Menten (Menten 1991), single-dish obs.		05:39:13.0 35:45:48.7	−17
18089−1732	18:11:51.4 −17:31:30.2[1]	39	18:11:51.5 −17:31:28.8	32
18090−1832	18:12:01.9 −18:31:55.0[1]	108		
18102−1800	18:13:11.3 −17:59:57.8	25		
	18:13:11.3 −17:59:58.0	24/23		
18151−1208	18:17:58.1 −12:07:25.4	28	18:17:50.3 −12:07:52.9	22/25/32
18182−1433	18:21:09.2 −14:31:48.6[1]	62	18:21:09.1 −14:31:48.7	60
			18:21:09.1 −14:31:47.8	65
			18:21:09.0 −14:31:48.5	57
			18:21:09.0 −14:31:47.9	50/53
			18:21:09.1 −14:31:48.6	68
18264−1152	18:29:14.4 −11:50:22.4	47	18:29:14.2 −11:50:22.6	45/52
			18:29:14.4 −11:50:24.5	61/68/74
			18:29:14.3 −11:50:22.5	52
18290−0924	18:31:44.2 −09:22:12.5[1]	80	18:31:44.1 −09:22:12.1	88
18306−0835			18:33:23.9 −08:33:31.6	105
			18:33:17.1 −08:33:24.3	82
18308−0841			18:33:33.2 −08:39:15.1	69/73/86
18310−0825	18:33:43.8 −08:21:20.5[1]	88		
18345−0641	18:37:16.9 −06:38:30.4	97		
	18:37:17.0 −06:38:30.3	94		
18372−0541	18:39:55.9 −05:38:45.1	25	18:39:55.9 −05:38:44.1	23
	18:39:55.9 −05:38:44.9	24	18:39:55.9 −05:38:44.6	26
	18:39:56.0 −05:38:45.9	23		
	18:39:56.0 −05:38:45.8	18		
18385−0521			18:41:13.2 −05:09:00.5	19
			18:41:13.2 −05:09:01.0	11
			18:41:13.2 −05:09:01.1	26
			18:41:13.2 −05:09:01.2	30
			18:41:13.2 −05:09:01.3	37
18440−0148	18:46:36.7 −01:45:22.2[1]	105		
18488+0000			18:51:24.5 00:04:33.7	80
18521+0134	18:54:40.8 01:38:04.5	77		
18553+0414			18:57:53.4 04:18:17.4	4
			18:57:53.4 04:18:17.3	12
18566+0408	18:59:10.0 04:12:14.7	87/86	18:59:10.0 04:12:15.6	88
	18:59:10.0 04:12:14.1	84	18:59:10.0 04:12:15.7	68
	18:59:10.0 04:12:14.0	79		
19012+0536			19:03:45.3 05:40:42.8	63
19035+0641	19:06:01.6 06:46:35.9	37/31	19:06:01.6 06:46:36.3	21
19217+1651	19:23:58.9 16:57:41.8	7	19:23:58.5 16:57:41.4	18
			19:23:58.8 16:57:41.5	11
			19:23:58.8 16:57:41.1	8
19282+1814	19:30:23.0 18:20:27.1	19		
19410+2336	19:43:11.3 23:44:03.3[2]	27	19:43:11.2 23:44:03.0	27
	19:43:11.2 23:44:03.0[2]	17	19:43:11.2 23:44:03.1	19
20126+4104	20:14:26.0 41:13:33.4[2]	−6	20:14:26.0 41:13:32.6	0
			20:14:26.0 41:13:32.7	−8
20293+3952			20:31:12.9 40:03:22.8	2/−28
23033+5951			23:05:25.0 60:08:14.1	−49/−55/−62
23139+5939			23:16:10.3 59:55:28.7	−48/−53
			23:16:10.3 59:55:28.6	−44
			23:16:10.4 59:55:28.8	−33
23151+5912			23:17:20.8 59:28:47.0	−52
			23:17:20.3 59:28:47.3	−69

Table 3. Separations of the CH_3OH masers from H_2O, mm, cm and mid-infrared sources. Far and near values correspond to the far and near distance, respectively. For sources without near values, the distance ambiguity is solved (Sridharan et al. 2002). The uncertainty of the CH_3OH/H_2O column is ∼1.5″ and scales with the distances for the linear separations. The uncertainties of the other columns are ∼5″, scaling with the distances as well.

source	CH_3OH/H_2O			CH_3OH/mm			CH_3OH/cm			CH_3OH/MIR		
		far	near		far	near		far	near		far	near
	[″]	[pc]	[pc]	[″]	[pc]	[pc]	[″]	[pc]	[pc]	[″]	[pc]	[pc]
18089−1732	1.5	0.1	0.03	1.5	0.1	0.03	1.5	0.1	0.03	11	0.69	0.19
18090−1832				0.5	0.02	0.02				0.5	0.02	0.02
18102−1800				4	0.27	0.05	30	2.04	0.38	30	2.04	0.38
18151−1208	80	1.16		0.5	0.01					12	0.16	
18182−1433	1	0.06	0.02	1	0.06	0.02				12	0.67	0.26
18264−1152	1	0.06	0.02	1	0.06	0.02				9	0.55	0.15
18290−0924	1	0.05	0.03	2	0.1	0.05	20	1.02	0.51	1	0.05	0.03
18310−0825				4	0.2	0.1				16	0.81	0.40
18345−0641				0.5	0.02					3	0.14	
18372−0541	0.5	0.03	0.004	1	0.07	0.01	1	0.07	0.01	1	0.07	0.01
18440−0148				1	0.04					4	0.16	
18521+0134				1	0.04	0.02				4	0.18	0.1
18566+0408	1	0.03		1	0.03					1	0.03	
19035+0641	0.5	0.01		2	0.02		7	0.08		1	0.01	
19217+1651	0.5	0.03		1	0.05		6	0.3		1.5	0.08	
19282+1814				1	0.04	0.01				20	0.80	0.18
19410+2336	0.5	0.02	0.01	5	0.16	0.05	1	0.03	0.01	5	0.16	0.05
20126+4104	1	0.01		1	0.01					3	0.03	

Table 4. Separations of the H_2O masers from mm, cm and mid-infrared sources. Far and near values correspond to the far and near distance, respectively. For sources without near values, the distance ambiguity is solved (Sridharan et al. 2002). The uncertainties are ∼5″, scaling with the distances for the linear separations.

source	H_2O/mm			H_2O/cm			H_2O/MIR		
		far	near		far	near		far	near
	[″]	[pc]	[pc]	[″]	[pc]	[pc]	[″]	[pc]	[pc]
05358+3543	2	0.02					3	0.03	
18089−1732	0.5	0.03	0.01	0.5	0.03	0.01	10	0.63	0.18
18151−1208	0.5	0.01							
18182−1433	1	0.06	0.02				12	0.67	0.26
18264−1152	1	0.06	0.02				7	0.67	0.26
18290−0924	2	0.1	0.01	20	1.02	0.51	1	0.05	0.03
18306−0835	0.5	0.03	0.01	12	0.62	0.29	12	0.62	0.29
18308−0841	4	0.2	0.1				7	0.36	0.17
18372−0541	1	0.07	0.01	1	0.07	0.01	1	0.07	0.01
18385−0512	1	0.06	0.01	3	0.19	0.03	1	0.06	0.01
18488+0000	4	0.17	0.11	20	0.89	0.54	3	0.13	0.08
18553+0414	1	0.06	0.003	18	1.13	0.05	3	0.19	0.01
18566+0408	0.5	0.02					1	0.02	
19012+0536	0.5	0.02	0.01				7	0.29	0.16
19035+0641	2	0.02		7	0.08		1	0.01	
19217+1651	1	0.05		6/1	0.3/0.05		2	0.1	
19410+2336	5	0.16	0.05	1	0.03	0.01	5	0.16	0.05
20126+4104	2	0.16					2	0.16	
20293+3952	2	0.19	0.13	18	0.18	0.11	22	0.21	0.14
23033+5951	1	0.02		1.5	0.03		4	0.07	
23139+5939	1	0.02		1	0.02		0.5	0.01	
23151+5912	1.5	0.04					7	0.19	

none of them has a coherent velocity structure and therefore cannot easily be interpreted in terms of disks, outflows or expanding shock waves. There is also no obvious correlation with the outflow direction. With only one set of observations, it is very difficult to interpret these morphological and kinematic signatures, but it is well possible that follow-up observations,

Table 5. Frequency of associated features within the spatial resolution as given in Sect. 3. The third column gives the percentage of associations with respect to the total number of sources where CH_3OH or H_2O masers were detected. The last column presents the mean separations and their uncertainties.

association	number	%	mean [pc]
CH_3OH/H_2O	10	56	0.02 ± 0.03
CH_3OH/mm	18	100	0.03 ± 0.10
CH_3OH/cm	3	17	0.19 ± 0.03
CH_3OH/MIR	11	61	0.13 ± 0.10
H_2O/mm	22	100	0.03 ± 0.10
H_2O/cm	6	27	0.13 ± 0.03
H_2O/MIR	13	59	0.09 ± 0.10

and thus proper motion studies, might be capable of setting better constraints on the regions where the maser emission is produced. Such studies were successful in a number of cases, e.g., Alcolea et al. (1992) and Minier et al. (2000b).

4. Discussion

The observations presented in Sect. 3 confirm that both maser species – CH_3OH and H_2O – are signposts of very early stages of massive star formation. While 100% of the maser detections are clearly associated with massive molecular cores traced by mm dust continuum emission, only about 20% are also associated with cm continuum emission that is indicative of recently ignited, and thus more evolved stars. These observations confirm results obtained for each maser species separately over the last few years, that CH_3OH and H_2O masers are signposts of very early stages of massive star formation, and that both seem to cease emission soon after the ignition of a central object (e.g., Tofani et al. 1995; Codella et al. 1996, 1997; Walsh et al. 1998; Minier et al. 2001). Here we show for the first time the similarities and differences of both maser types within a consistent study of a homogenous sample.

In spite of the small separations around 0.03 pc within many sources, there are clear differences between both maser types. In addition to their large velocity differences (Sridharan et al. 2002), in approximately 30% of the sources just one maser species is found. We do find a few sources with nearby H_2O maser and cm emission, but not showing CH_3OH maser emission. In contrast, every source, where CH_3OH maser emission is associated with a cm source, has an H_2O maser nearby. This difference suggests tentatively that CH_3OH maser emission might be more sensitive to the ignited central object, and may cease emitting in somewhat earlier evolutionary stages than H_2O maser emission. However, it has to be noted that counterexamples exist, e.g., the W3(OH) region, where the CH_3OH masers are associated with the ultracompact HII region, and the H_2O masers are approximately 6″ to the east associated with the hot core W3(H_2O). For a summary of the results in that region see Menten (1996).

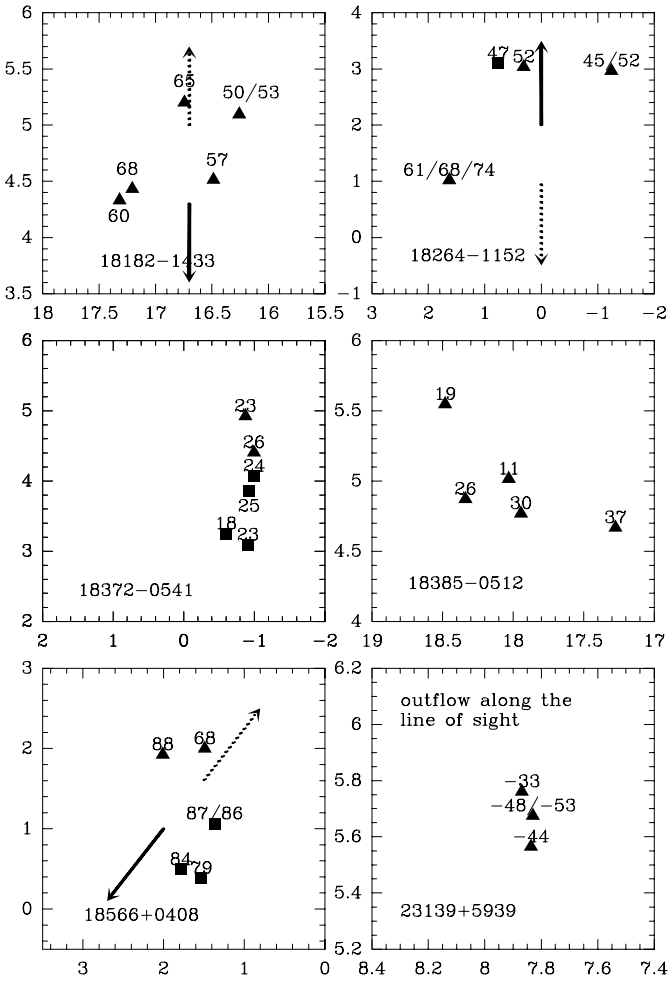

Fig. 2. Zoom into some maser distributions. The triangles show H_2O masers and the squares CH_3OH masers. The numbers mark the radial velocities at which each feature emits, and the arrows indicate the overall directions of the molecular outflows (solid: blue wing, dashed: red wing) as found by Beuther et al. (2002b). The axes show the offsets in arcseconds from the IRAS position.

CH_3OH maser models propose that the maser emission is produced by radiative pumping in moderately hot regions (~150 K) with CH_3OH column densities $>2 \times 10^{15}$ cm^{-2} and hydrogen number densities $<10^8$ cm^{-3} (Hartquist et al. 1995; Sobolev et al. 1997; Cragg et al. 2001). The data presented here as well as other studies (e.g., Walsh et al. 1997; 1998; Phillips et al. 1998; Minier et al. 2000a; 2001) indicate that the ignition of a massive star, and thus the formation of an ultracompact HII region, alters these conditions swiftly and stops further CH_3OH maser emission very soon.

In contrast, H_2O maser models mostly explain the excitation by collisional pumping with H_2 molecules in shocks associated with outflows (Elitzur et al. 1989). Such collisional pumping can also occur by accretion shocks in accretion disks (Garay & Lizano 1999). These processes may not depend as strongly on the influence of the HII region as the radiative pumping of the CH_3OH maser, and H_2O maser emission might continue some time in more evolved stages of evolution. But

obviously, the statistics of the observations are not sufficient for a stronger statement.

The percentage of associated maser and mid-infrared sources (~60%) lies in a similar regime as found recently by Walsh et al. (2001). They propose that the mid-infrared objects, which are likely to be embedded luminous protostellar objects, could be the pumping sources of the maser sites. This might be true in the associated sources of our sample as well, but the percentage of associations clearly shows that detections in the mid-infrared regime are not necessary to produce the maser emission. It is possible that for high obscuration the sources are not detectable in the mid-infrared – only the maser shows up.

Additionally, we do not find strong correlations between the spatial separations of the different observed quantities and other characteristic quantities of the sources, e.g., the luminosities, core masses, column densities, and volume densities. Thus, it seems likely that both maser species need a similar environment of dense and warm gas, but that, due to the different excitation processes (radiative pumping for CH_3OH and collisional pumping for H_2O), no real correlation exists. Spatial associations of both maser species might be just coincidences caused by insufficient spatial resolution and projection effects.

We cannot determine accurately in any source of this sample whether the maser emission is produced in disks, outflows or shock waves. This stresses that kinematic interpretations of different maser features are difficult and not as straightforward as sometimes supposed in the past (e.g., Garay & Lizano 1999; Norris et al. 1998). CH_3OH and H_2O masers are excellent signposts of massive star-forming regions, but the detailed interpretation of the different kinematic and spatial features has to be treated with caution. There are definitely cases where the kinematic information gives deep insights in special sources, e.g., the H_2O maser in W3(H_2O) (Alcolea et al. 1992), or some of the linear structures found in CH_3OH by, e.g., Walsh et al. (1998), Minier et al. (2000a), Norris et al. (1998), and Phillips et al. (1998), but as stressed by Minier et al. (2000a), proper motions and VLBI observations are needed to derive conclusive answers for such sources. We believe that the approach of kinematic interpretation of different maser features works only in a limited number of sources with a favorable geometry with respect to the observer, and then especially when proper motion observations are available. With this regard, the data presented in this paper are a well suited basis for follow-up proper motion studies of both maser species. Except for this, for most sources, the main and highly important outcome of maser observations in massive star-forming regions is their characteristics as signposts for high-mass star formation.

Acknowledgements. We like to thank the referee Dr. G. Fuller for detailed comments on the first draft, which improved the quality of the paper significantly. H. Beuther got support by the *Deutsche Forschungsgemeinschaft, DFG* project number SPP 471.

References

Alcolea, J., Menten, K. M., Moran, J., & Reid, M. J. 1992, in Astrophysical Masers, ed. A. W. Clegg, & G. E. Nedoluha (Springer, Berlin), 225
Beuther, H., Sridharan, T. K., Schilke, P., Menten, K. M., & Wyrowski, F. 2002a, ApJ, 566, 945
Beuther, H., Sridharan, T. K., Schilke, P., et al. 2002b, A&A, 383, 892
Beuther, H., Schilke, P., Gueth, F., Menten, K. M., & Sridharan, T. K. 2002c, A&A, 387, 931
Bonnell, I., Bate, M., & Zinnecker, H. 1998, MNRAS, 298, 93
Churchwell, E. 2000, in The Origins of Stars and Planetary Systems, ed. C. J. Lada, & N. D. Kylafis (Kluwer Academic Press)
Codella, C., & Felli, M. 1995, A&A, 302, 521
Codella, C., Felli, M., & Natale, V. 1996, A&A, 311, 971
Codella, C., Testi, L., & Cesaroni, R. 1997, A&A, 325, 282
Codella, C., & Moscadelli, L. 2000, A&A, 362, 723
Cragg, D. M., Sobolev, A. M., Ellingsen, S. P., et al. 2001, MNRAS, in press
Egan, M. P., Shipman, R. F., Price, S. D., Carey, S. J., & Clark, F. O. 1998, ApJ, 494, L199
Elitzur, M., Hollenbach, D. J., & McKee, C. F. 1989, ApJ, 346, 983
Garay, G., & Lizano, S. 1999, PASP, 111, 1049
Hartquist, T. W., Menten, K. M., Lepp, S., & Dalgarno, A. 1995, MNRAS, 272, 184
Hofner, P., & Churchwell, E. 1996, A&AS, 120, 283
Kylafis, N. D., & Pavlakis, K. G. 1999, in The Origins of Stars and Planetary Systems, ed. C. J. Lada, & N. D. Kylafis (Kluwer Academic Press)
Lada, E. A. 1999, in The Origins of Stars and Planetary Systems, ed. C. J. Lada, & N. D. Kylafis (Kluwer Academic Press)
Massey, P. 1998, in The Stellar Initial Mass function, ASP Conf. Ser., 142, ed. G. Gilmore, & D. Howell
Menten, K. 1991, ApJ, 380, L75
Menten, K. M. 1996, in IAU Symp., 178, ed. E. van Dishoek
McCaughrean, M., & Stauffer, J. 1994, AJ, 108, 1382
Minier, V., Booth, R. S., & Conway, A. G. 2000a, A&A, 362, 1093
Minier, V., Booth, R. S., Ellingsen, S. P., Conway, J. E., & Pestalozzi, M. R. 2000b, in Proceedings of the 5th EVN Symposium, Convay, J., Polatidis, A., & Booth, R. (eds.), Chalmers Technical University, Githenburg, Sweden
Minier, V., Conway, A. G., & Booth, R. S. 2001, A&A, 369, 278
Norris, R. P., Byleveld, S. E., Diamond, P. J., et al. 1998, ApJ, 508, 275
Norris, R. P. 2000, in IAU Symposium 197, ed. Y. C. Minh, & E. F. van Dishoek, Astronomical Society of the Pacific Conference Series
Phillips, C. J., Norris, R. P., Ellingsen, S. P., & McCulloch, P. M. 1998, MNRAS, 300, 1131
Preibisch, Th., Balega, Y., Hofmann, K.-H., Weigelt, G., & Zinnecker, H. 1999, New Astron., 4, 531
Richer, J., Shepherd, D., Cabrit, S., Bachiller, R., & Churchwell, E. 2000, in Protostars & Planets IV, ed. V. Mannings
Sobolev, A. M., Cragg, D. M., & Godfrey, P. D. 1997, A&A, 324, 211
Sridharan, T. K., Beuther, H., Schilke, P., Menten, K., & Wyrowski, F. 2002, ApJ, 566, 931
Stahler, S., Palla, F., & Ho, P. 2000, in Protostars & Planets IV (The University of Arizona Press)
Tofani, G., Felli, M., Taylor, G., & Hunter, T. 1995, A&AS, 112, 299
Torrelles, J. M., Gomez, J. F., Rodriguez, L. F., Ho, P. T. P., et al. 1997, ApJ, 489, 744
Torrelles, J. M., Gomez, J. F., Garay, G., et al. 1998, ApJ, 509, 262
Walsh, A. J., Hyland, A. R., Robinson, G., & Burton, M. G. 1997, MNRAS, 291, 261
Walsh, A. J., Burton, M. G., Hyland, A. R., & Robinson, G. 1998, MNRAS, 301, 640
Walsh, A. J., Bertoldi, F., Burton, M. G., & Nikola, T. 2001, MNRAS, 326, 36